GEOPHYSICAL RESEARCH LETTERS, VOL. 40, 5637–5641, doi:10.1002/2013GL057884, 2013

Water retention curve for hydrate-bearing sediments

Sheng Dai[1] and J. Carlos Santamarina[1]

Received 3 September 2013; revised 11 October 2013; accepted 15 October 2013; published 4 November 2012.

[1] The water retention curve plays a central role in numerical algorithms that model hydrate dissociation in sediments. The determination of the water retention curve for hydrate-bearing sediments faces experimental difficulties, and most studies assume constant water retention curves regardless of hydrate saturation. This study employs network model simulation to investigate the water retention curve for hydrate-bearing sediments. Results show that (1) hydrate in pores shifts the curve to higher capillary pressures and the air entry pressure increases as a power function of hydrate saturation; (2) the air entry pressure is lower in sediments with patchy rather than distributed hydrate, with higher pore size variation and pore connectivity or with lower specimen slenderness along the flow direction; and (3) smaller specimens render higher variance in computed water retention curves, especially at high water saturation $S_w > 0.7$. Results are relevant to other sediment pore processes such as bioclogging and mineral precipitation. **Citation:** Dai, S., and J. C. Santamarina (2013), Water retention curve for hydrate-bearing sediments, *Geophys. Res. Lett.*, *40*, 5637–5641, doi:10.1002/2013GL057884.

1. Introduction

[2] The development of governing equations for unsaturated sediments has centered on the saturation-dependent capillary pressure, also known as the water retention curve, soil water characteristic curve, or soil suction versus volumetric water content curve [*Brady and Weil*, 2007; *Fredlund and Rahardjo*, 1993; *Jury et al*., 1991; *Kovács*, 2011; *Lu and Likos*, 2004]. The water retention curve of a soil is inherently determined by pore-scale characteristics including pore shape and size distribution, interconnectivity and spatial variability, fluids and interfacial tension, mineral type, and fluid-mineral interactions captured in the contact angle and hysteresis [*Aubertin et al*., 2003; *Francisca and Arduino*, 2007; *Huang et al*., 2006; *Perrier et al*., 1996].

[3] Measured suction-saturation curves are relatively smooth and can be fitted with simple functions of two or three parameters that typically capture the air entry pressure P_0 and the sensitivity of changes in saturation S_w to changes in capillary pressure P_c, i.e., the curve slope $\partial S_w/\partial P_c$ [*Brooks and Corey*, 1964; *Corey*, 1954; *Farrell and Larson*, 1972; *Fredlund and Xing*, 1994; *Gardner*, 1958; *Kosugi*, 1994; *van Genuchten*, 1980]. Empirical models relate the water retention curve (i.e., P_0 and slope parameters) to basic sediment properties, such as grain size distribution, bulk density, and porosity [*Arya and Paris*, 1981; *Assouline*, 2006; *Aubertin et al*., 2003; *Chiu et al*., 2012; *Haverkamp and Parlange*, 1986; *Stange and Horn*, 2005].

[4] The water retention curve is causally linked to all the physical properties of unsaturated sediments, such as relative permeability [*Assouline*, 2001; *Campbell*, 1974; *Fischer and Celia*, 1999; *Mualem*, 1986; *Vogel and Cislerova*, 1988], storage and field capacity [*Brady and Weil*, 2007], shear strength [*Fredlund et al*., 1996; *Öberg and Sällfors*, 1997; *Vanapalli et al*., 1996], stiffness, and volume change [*Delage et al*., 1998; *Gens and Alonso*, 1992; *Pedarla et al*., 2012]. Therefore, most numerical codes for coupled processes in unsaturated sediments are anchored on the water retention curve, including CODE-BRIGHT [*Olivella et al*., 1994] and TOUGH + HYDRATE [*Moridis et al*., 2008].

[5] The water retention curve is measured by applying a pressure difference between the two fluids involved, either using vacuum, excess pressure, controlled suction, or relative humidity. The volume fraction of either the wetting or the nonwetting fluid is measured at equilibrium at each capillary pressure (reviews in *Barbour* [1998], *Fredlund and Rahardjo* [1993], and *Lu and Likos* [2004]).

[6] Numerical simulation results show that the behavior of hydrate-bearing reservoirs is strongly linked to the water retention curve [*Kimoto et al*., 2007; *Sanchez and Santamarina*, 2010]. Yet the water retention curve is assumed constant regardless of hydrate saturation in most cases [*Hong and Pooladi-Darvish*, 2005; *Kimoto et al*., 2007; *Moridis et al*., 2011; *Moridis and Sloan*, 2007; *Reagan and Moridis*, 2008; *Uddin et al*., 2011]. In part, this is due to lack of data: The determination of the water retention curve for hydrate-bearing sediments is experimentally challenging as it must involve high fluid pressure and low temperature to prevent hydrate dissociation.

[7] Pore network model simulations reproduce pore-scale processes and provide the macroscale sediment response [*Blunt*, 2001; *Fatt*, 1956], such as the evolution of unsaturation and resulting water retention curves [*Fischer and Celia*, 1999; *Peat et al*., 2000; *Vogel*, 2000]. This study uses network model simulations to investigate the capillarity-saturation response in hydrate-bearing sediments.

2. The Water Retention Curve of Hydrate-Bearing Sediments

[8] The sediment porous network is represented as a lattice of tubes with identical length L_t and varying radius r in network model simulation. Tubes are connected at zero-volume nodes; hence, the total pore space is the sum of the volume of tubes. The number of tubes connected at a node is the pore connectivity cn. Mercury intrusion porosimetry data show that natural sediments exhibit a lognormal distribution in

Additional supporting information may be found in the online version of this article.

[1]School of Civil and Environmental Engineering, Georgia Institute of Technology, Atlanta, Georgia, USA.

Corresponding author: S. Dai, School of Civil and Environmental Engineering, Georgia Institute of Technology, Atlanta, GA 30332, USA. (sheng.dai@gatech.edu)

0094-8276/13/10.1002/2013GL057884

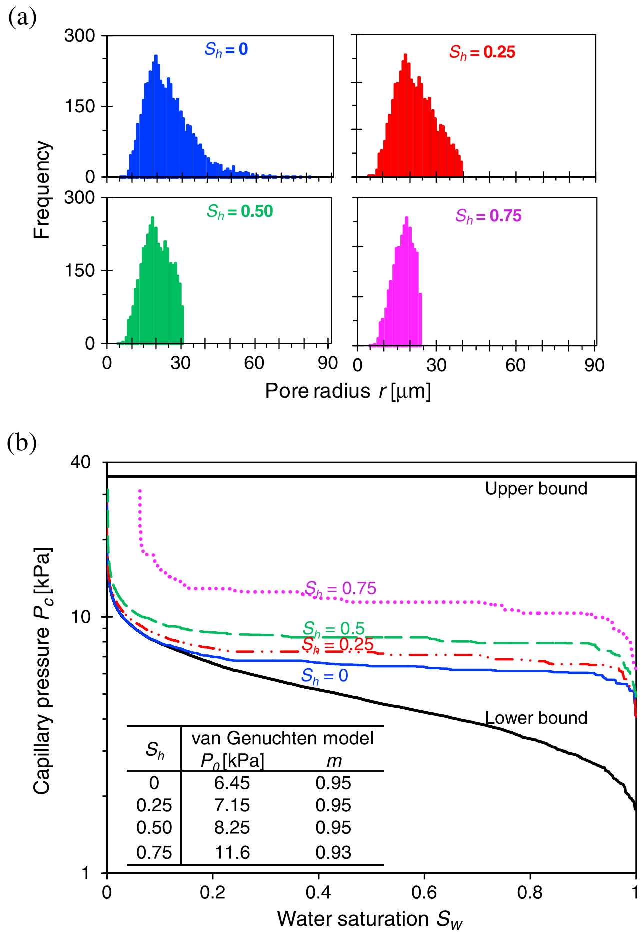

Figure 1. Water retention curves for sediments with different hydrate saturations S_h. (a) Change in pore size distribution as a function of hydrate saturation, assuming that the hydrate mass fills the largest pores first. (b) Computed water retention curves using preformed 2-D networks ($cn=4$) as a function of hydrate saturation S_h (Note: Hydrate forms in the largest pores). Numerical results are fitted using van Genuchten model, where the reference pressure P_0 reflects the air entry pressure and the m parameter captures the sensitivity of changes in capillary pressure P_c to changes in water saturation S_w. Pore size statistics $\mu_{(\ln r/1\ \mu m)}=10$, $\sigma_{(\ln r/1\ \mu m)}=0.4$.

pore size with standard deviation $\sigma_{(\ln r/1\ \mu m)}=0.4\pm0.2$ [*Phadnis and Santamarina*, 2011]. In this study, pore radii are randomly generated to satisfy a lognormal distribution.

[9] Air invades the largest boundary-connected tube first as it mobilizes the lowest air entry pressure $P_c=2T_s\cos\theta/r$, where the air-water interfacial tension is $T_s=0.072$ N/m and contact angle is assumed $\theta=0°$ for a perfectly wetting system. All tubes exposed to the gas phase are potential candidates for further gas invasion. Air invasion displaces water and reduces the water saturation to $S_w=1-V_{in}/V_t$, where V_{in} is the volume of gas-invaded tubes and the total volume of pores is $V_t=\Sigma(\pi r^2 L_t)$. These steps are repeated to eventually define the variation in capillary pressure P_c and water saturation S_w. We note that the upper and lower bounds of the water retention curve can be obtained by invading all tubes arranged in series forming a single line from smallest to largest (upper bound) or in parallel (lower bound—Figure S1 in the supporting information).

[10] Water retention curves computed using network model simulations (see more details in Text S1 in the supporting information) are quantitatively described using the *van Genuchten* [1980] model to capture the dependence of capillary pressure P_c on water saturation S_w

$$P_c = P_0\left[\left(\frac{S_w-S_r}{1-S_r}\right)^{-\frac{1}{m}}-1\right]^{1-m} \tag{1}$$

where P_0 reflects the air entry value (Note: The "physical air entry pressure" is the air-water pressure difference needed to invade the largest pore on a soil specimen surface; the value P_0 used herein is a generic fitting parameter in the van Genuchten model), m value captures the sensitivity of water saturation S_w to capillarity P_c, and S_r is the residual water saturation. Once the m value is known, the *Brooks and Corey* [1964] and *van Genuchten* [1980] models can be used to compute relative permeabilities for water and gas.

2.1. Hydrate Saturation

[11] Hydrate forms in pores, shuts flow paths, and alters the water retention curve. As hydrate growth is inhibited in smaller pores size < 100 nm [*Clennell et al.*, 1999; *Kwon et al.*, 2008; *Malinverno*, 2010], hydrates are assumed to fill the largest tubes first (Note: Other hydrate pore-filling habits are considered in the next section). Figure 1a shows the histogram for 4802 pore with lognormally distributed size ($\mu_{(\ln r/1\ \mu m)}=10$ and $\sigma_{(\ln r/1\ \mu m)}=0.4$); the other three histograms correspond to hydrate-free pores and are computed from the first histogram by assuming the largest tubes are plugged by hydrates to reach hydrate saturations $S_h=0.25$, 0.5, and 0.75.

[12] Computed water retention curves shift to higher capillary pressure as hydrate fills the largest pores and gas invasion is limited to smaller hydrate-free pores (Figure 1b). The trend between hydrate saturation S_h and air entry pressure P_0^{HBS} is studied using multiple realizations for different hydrate saturations S_h. The porous medium gradually shuts off as the hydrate saturation approaches $S_h\sim0.8$. Water retention curves are fitted by adjusting P_0 and m values: The air entry pressure P_0 increases with hydrate saturation, but the m value remains relatively constant until hydrate saturations exceed $S_h>0.5$ (see the inset of Figure 1b and Text S2). The hydrate saturation-dependent entry value P_0 for hydrate-bearing sediments follows a power equation:

$$\frac{P_0^{HBS}}{P_0^{HF}} = \left(\frac{0.8}{0.8-S_h}\right)^{0.25} \quad \text{for } S_h<0.8 \tag{2}$$

where P_0^{HF} is the air entry pressure for hydrate-free sediments; percolating water path shuts off when $S_h\approx0.8$ (refer to Figure 1b). Pressure normalization with respect to the hydrate-free network extends the validity of this trend to a wide range of sediments. Note that these results apply for a pore size variability $\sigma_{(\ln r/1\ \mu m)}\approx0.4$. Computed capillary pressures scale linearly with *PT*-dependent surface tension and contact angle in each tube. Therefore, normalized curves P/P_0 apply throughout a reservoir as long as local *PT* conditions are taken into consideration. (Note: The validity to sediments with different pore size variability requires further validation).

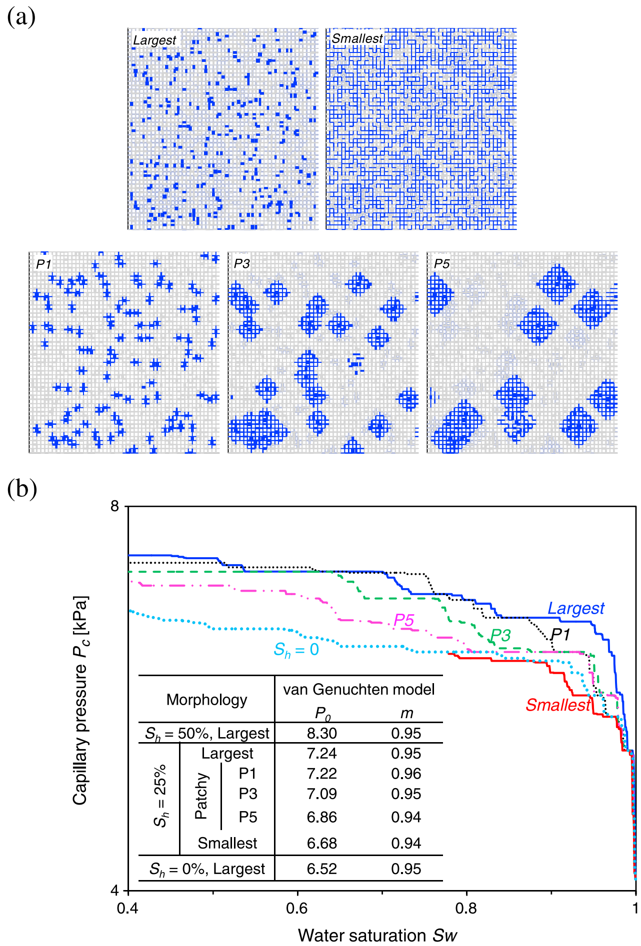

Figure 2. The effect of hydrate morphology on the water retention curve using identical tube networks. (a) The same hydrate saturation $S_h = 25\%$ is satisfied with five different pore habits: Hydrate forms in either the largest or the smallest tubes, or in patches of different patch size (*P1*, *P3*, and *P5*) that preferentially nucleate at the largest pores.(b) Corresponding soil water characteristic curves and fitted van Genuchten model parameters. Pore size statistics $\mu_{(\ln r/1\ \mu m)} = 10$, $\sigma_{(\ln r/1\ \mu m)} = 0.4$.

2.2. Hydrate Pore-Filling Topology

[13] Hydrate growth is thermodynamically preferred over hydrate nucleation at new sites. Such nucleation-growth preferences affect the spatial distribution of hydrates in sediments. Let us consider sediments with identical hydrate saturation $S_h = 0.25$ but different hydrate topologies (Figure 2a): Hydrate fills the largest tubes or the smallest tubes (albeit physically unlikely), or hydrate forms patches, whereby hydrate nucleates in the largest tubes and grows into neighboring tubes up to one-grid, three-grid, or five-grid distances (*P1*, *P3*, and *P5* in Figure 2a—this topology is favored by Ostwald ripening [*Dai et al*., 2012]).

[14] The computed water retention curves are shown in Figure 2b. The upper curve corresponds to disseminated hydrate filling the largest tubes. The water retention curve for hydrate filling the smallest pores resembles the curve for hydrate-free $S_h = 0$ sediment, and it is the lower bound for these trends. The larger the patch size, the lower the air entry pressure P_0, as many relatively large tubes remain hydrate free in patchy saturation. Fitted van Genuchten trends show that hydrate morphology affects both the air entry pressure P_0 and the slope m value.

3. Discussion

[15] Network model simulation allows us to explore the effects of pore characteristics such as pore size statistics and pore connectivity on the water retention curve (Note: The effect of specimen size and geometry that affects both numerical studies as well as the experimental determination of the water retention curve is investigated in Text S3).

3.1. Pore Size Statistics

[16] The effect of pore size variability on the water retention curve is explored using three sets of lognormally distributed pores with identical mean pore size $\mu_{(\ln r/1\ \mu m)}$ but different standard deviations $\sigma_{(\ln r/1\ \mu m)}$ (Figure 3a). Water retention curves shown in Figure 3b suggest that a larger variation in sediment pore size reduces both the air entry pressure P_0 and the slope m value. The capillary pressure $P_c = 2T_s/r$ at a water saturation $S_w = 0.9$ corresponds approximately to the

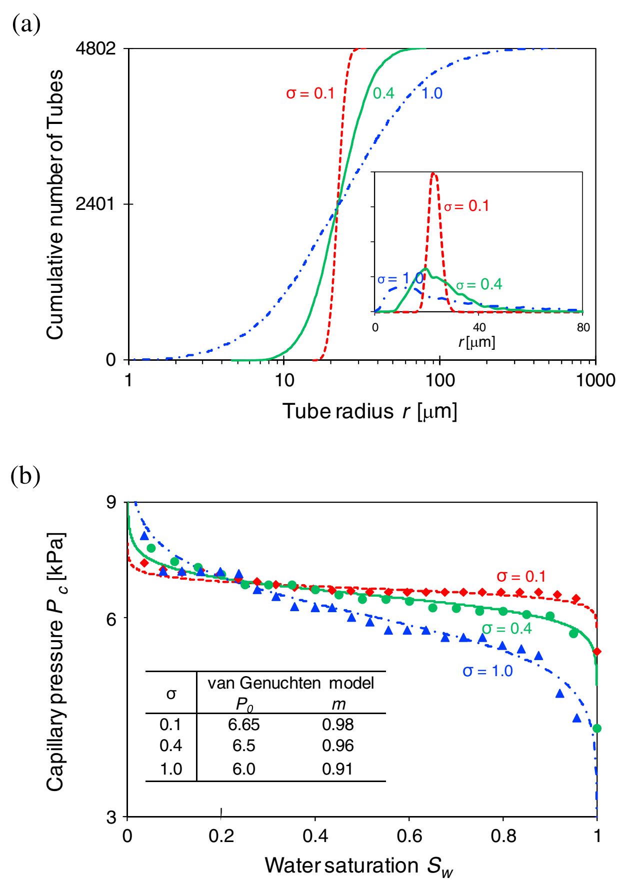

Figure 3. The effect of pore size statistics on the water retention curve (Note: hydrate saturation $S_h = 0\%$). (a) Lognormal pore size distributions with identical mean $\mu_{(\ln r/1\ \mu m)}$ but different standard deviations $\sigma_{(\ln r/1\ \mu m)}$. The inset shows the corresponding density curves. (b) Network model simulation results (markers) and fitted van Genuchten model (lines).

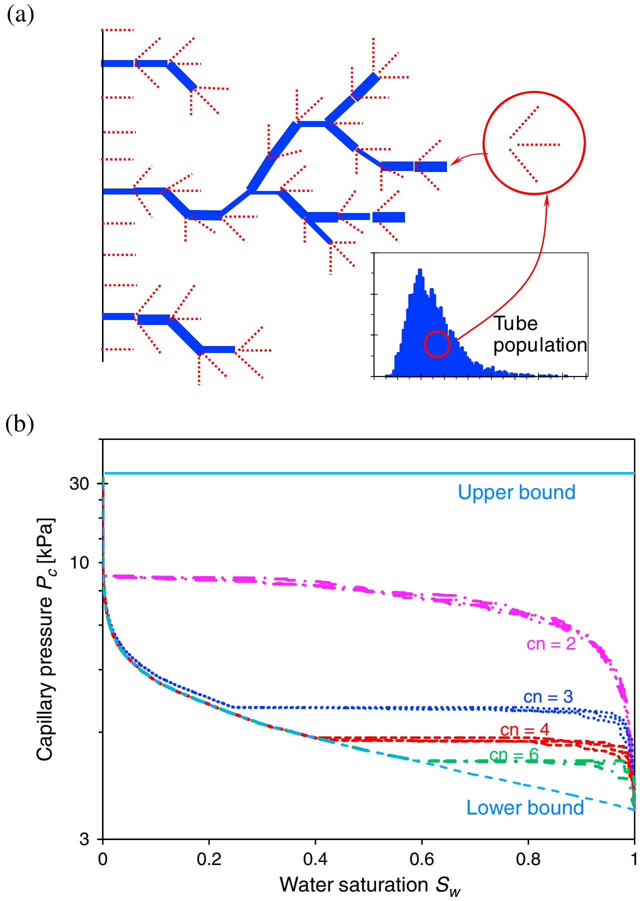

Figure 4. Concurrent invasion and growth algorithm for the study of pore connectivity. (a) Illustration of random network growth: Solid lines are gas-invaded tubes; new tubes (dashed lines) are randomly selected from the total tube population and connected to the newly gas-invaded tube, until all tubes in the population are exhausted. (b) Water retention curves for network realizations with different pore connectivity *cn* (Note: Refer to Figure S1 for the tube population—$S_h = 25\%$ hydrate clogs the largest pores).

mean pore size $\mu_{(r/1\ \mu\mathrm{m})} = \sum_1^n r_i / n$ in all cases (Note: This is not the mean of the natural log of pore size $\mu_{(\ln r/1\ \mu\mathrm{m})} = \sum_1^n (\ln r_i)/n$). In other words, the pressure required for the initiation of decisive gas invasion is determined by the sediment mean pore size.

3.2. Pore Coordination

[17] The 2-D square network used for studies reported above has a constant pore coordination $cn = 4$. Yet pore connectivity higher than $cn = 4$ can be observed in 3-D porous media. The effect of coordination number is tested using a concurrent invasion and growth algorithm: Instead of preforming a fixed network, the network grows simultaneously with air invasion by randomly selecting tubes from the tube population (details in Text S4).

[18] Results obtained using the concurrent invasion and growth algorithm for different pore connectivity show that water retention curves exhibit lower air entry pressure as the pore coordination increases (Figure 4b).

4. Conclusions

[19] The water retention curve captures the association between capillary pressure and water saturation, and it is inherently determined by sediment pore-scale characteristics, such as pore size distribution and connectivity. The water retention curve plays a central role in reservoir simulations.

[20] Preferential hydrate nucleation in larger pores leaves statistically smaller pores available for gas invasion. The air entry pressure P_0 increases with hydrate saturation S_h, yet the slope of the water retention curve remains relatively constant.

[21] Percolating water flow paths shut off when hydrate saturation approaches S_h ~80% if preferential hydrate nucleation takes place in large pores. Patchy hydrate distribution renders lower air entry pressure than distributed hydrate saturation.

[22] The air entry pressure of hydrate-bearing sediments P_0^{HBS} can be estimated from the air entry pressure of hydrate-free sediments P_0^{HF} as a power function of hydrate saturation.

[23] Higher variation in sediment pore size distribution and higher pore connectivity lower the air entry value P_0 but steepen the water retention curve. Decisive water displacement starts when the capillary pressure exceeds the capillary pressure for the mean pore size $\mu_{(r/1\ \mu\mathrm{m})}$.

[24] The specimen size and geometry bias the measured capillary pressure-saturation curve, especially at high water saturation when $S_w > 0.7$ (shown in Text S3). Smaller specimens produce higher variance in computed water retention curves. The air entry pressure increases with increasing specimen slenderness along the flow direction. Therefore, water retention curves determined in the laboratory should be applied with caution in reservoir simulations.

[25] These results and observations are relevant to a wide range of natural conditions including sediments that have experienced diagenesis, bioclogging, or mineral precipitation.

[26] **Acknowledgments.** Research support was provided by the Department of Energy/Joint Industry Project for methane hydrate, administered by Chevron. Additional funding was provided by the Goizueta Foundation.
[27] The Editor thanks two anonymous reviewers for their assistance in evaluating this paper.

References

Arya, L. M., and J. F. Paris (1981), A physicoempirical model to predict the soil moisture characteristic from particle-size distribution and bulk density data, *Soil Sci. Soc. Am. J.*, *45*(6), 1023–1030.
Assouline, S. (2001), A model for soil relative hydraulic conductivity based on the water retention characteristic curve, *Water Resour. Res.*, *37*(2), 265–271.
Assouline, S. (2006), Modeling the relationship between soil bulk density and the water retention curve contribution of the agricultural research organization, Institute of Soil, Water and Environmental Sciences, Bet Dagan, Israel, No. 607/05, *Vadose Zone J.*, *5*(2), 554–563.
Aubertin, M., M. Mbonimpa, B. Bussière, and R. P. Chapuis (2003), A model to predict the water retention curve from basic geotechnical properties, *Can. Geotech. J.*, *40*(6), 1104–1122.
Barbour, S. L. (1998), Nineteenth Canadian Geotechnical Colloquium: The soil-water characteristic curve: A historical perspective, *Can. Geotech. J.*, *35*(5), 873–894.
Blunt, M. J. (2001), Flow in porous media—Pore-network models and multiphase flow, *Curr. Opin. Colloid Interface Sci.*, *6*(3), 197–207.
Brady, N. C., and R. R. Weil (2007), *The Nature and Properties of Soils*, 14th ed., Pearson Prentice Hall, Upper Saddle River, N. J.
Brooks, R. H., and A. T. Corey (1964), Hydraulic properties of porous media, *Hydrology Papers, No.3*, Colorado State University, Fort Collins, Colo.
Campbell, G. S. (1974), A simple method for determining unsaturated conductivity from moisture retention data, *Soil Sci.*, *117*(6), 311–314.

Chiu, C. F., W. M. Yan, and K.-V. Yuen (2012), Estimation of water retention curve of granular soils from particle-size distribution—A Bayesian probabilistic approach, *Can. Geotech. J.*, *49*(9), 1024–1035.

Clennell, B. M., M. Hovland, J. S. Booth, P. Henry, and W. J. Winters (1999), Formation of natural gas hydrates in marine sediments: 1. Conceptual model of gas hydrate growth conditioned by host sediment properties, *J. Geophys. Res.*, *104*(B10), 22,985–23,003.

Corey, A. T. (1954), The interrelation between gas and oil relative permeabilities, *Producers Mon.*, *19*(1), 38–41.

Dai, S., J. C. Santamarina, W. F. Waite, and T. J. Kneafsey (2012), Hydrate morphology: Physical properties of sands with patchy hydrate saturation, *J. Geophys. Res.*, *117*, B11205, doi:10.1029/2012JB009667.

Delage, P., M. Howat, and Y. Cui (1998), The relationship between suction and swelling properties in a heavily compacted unsaturated clay, *Eng. Geol.*, *50*(1), 31–48.

Farrell, D. A., and W. E. Larson (1972), Modeling the pore structure of porous media, *Water Resour. Res.*, *8*(3), 699–706.

Fatt, I. (1956), The network model of porous media I. Capillary pressure characteristics, *Trans. AIME*, *207*(7), 144–159.

Fischer, U., and M. A. Celia (1999), Prediction of relative and absolute permeabilities for gas and water from soil water retention curves using a pore-scale network model, *Water Resour. Res.*, *35*(4), 1089–1100.

Francisca, F., and P. Arduino (2007), Immiscible displacement model for anisotropic and correlated porous media, *Int. J. Geomech.*, *7*(4), 311–317.

Fredlund, D. G., and A. Xing (1994), Equations for the soil-water characteristic curve, *Can. Geotech. J.*, *31*(4), 521–532.

Fredlund, D. G., and H. Rahardjo (1993), *Soil Mechanics for Unsaturated Soils*, Wiley, Hoboken, N. J.

Fredlund, D. G., A. Xing, M. D. Fredlund, and S. L. Barbour (1996), The relationship of the unsaturated soil shear to the soil-water characteristic curve, *Can. Geotech. J.*, *33*(3), 440–448.

Gardner, W. (1958), Some steady state solutions of the unsaturated moisture flow equation with application to evaporation from a water table, *Soil Sci.*, *85*(4), 228–232.

Gens, A., and E. Alonso (1992), A framework for the behaviour of unsaturated expansive clays, *Can. Geotech. J.*, *29*(6), 1013–1032.

Haverkamp, R., and J.-Y. Parlange (1986), Predicting the water-retention curve from particle-size distribution: 1. Sandy soils without organic matter, *Soil Sci.*, *142*(6), 325–339.

Hong, H., and M. Pooladi-Darvish (2005), Simulation of depressurization for gas production from gas hydrate reservoirs, *J. Can. Pet. Technol.*, *44*(11), 39–46.

Huang, G.-H., R.-D. Zhang, and Q.-Z. Huang (2006), Modeling soil water retention curve with a fractal method, *Pedosphere*, *16*(2), 137–146.

Jury, W. A., W. R. Gardner, and W. H. Gardner (1991), *Soil Physics*, Wiley, Hoboken, N. J.

Kimoto, S., F. Oka, T. Fushita, and M. Fujiwaki (2007), A chemo-thermo-mechanically coupled numerical simulation of the subsurface ground deformations due to methane hydrate dissociation, *Comput. Geotech.*, *34*(4), 216–228.

Kosugi, K. (1994), Three-parameter lognormal distribution model for soil water retention, *Water Resour. Res.*, *30*(4), 891–901.

Kovács, G. (2011), *Seepage Hydraulics*, Elsevier Science, Amsterdam.

Kwon, T.-H., G.-C. Cho, and J. C. Santamarina (2008), Gas hydrate dissociation in sediments: Pressure-temperature evolution, *Geochem. Geophys. Geosyst.*, *9*, Q03019, doi:10.1029/2007GC001920.

Lu, N., and W. J. Likos (2004), *Unsaturated Soil Mechanics*, Wiley, Hoboken, N. J.

Malinverno, A. (2010), Marine gas hydrates in thin sand layers that soak up microbial methane, *Earth Planet. Sci. Lett.*, *292*(3), 399–408.

Moridis, G. J., and E. D. Sloan (2007), Gas production potential of disperse low-saturation hydrate accumulations in oceanic sediments, *Energy Conversion Manage.*, *48*(6), 1834–1849.

Moridis, G. J., M. B. Kowalsky, and K. Pruess (2008), TOUGH +HYDRATE v1. 0 user's manual: A code for the simulation of system behavior in hydrate-bearing geologic media, *Report LBNL-00149E*, Lawrence Berkeley National Laboratory, Berkeley, Calif.

Moridis, G., S. Silpngarmlert, M. Reagan, T. Collett, and K. Zhang (2011), Gas production from a cold, stratigraphically-bounded gas hydrate deposit at the Mount Elbert Gas Hydrate Stratigraphic Test Well, Alaska North Slope: Implications of uncertainties, *Mar. Pet. Geol.*, *28*(2), 517–534.

Mualem, Y. (1986), Hydraulic conductivity of unsaturated soils: Prediction and formulas, in *Methods of Soil Analysis. Part I. Physical and Mineralogical Methods*, edited by A. Klute, pp. 799–823, American Society of Agronomy, Madison, Wisc.

Öberg, A.-L., and G. Sällfors (1997), Determination of shear strength parameters of unsaturated silts and sands based on the water retention curve, *ASTM Geotech. Test. J.*, *20*(1), 40–48.

Olivella, S., J. Carrera, A. Gens, and E. Alonso (1994), Nonisothermal multiphase flow of brine and gas through saline media, *Transport Porous Media*, *15*(3), 271–293.

Peat, D. M. W., G. P. Matthews, P. J. Worsfold, and S. C. Jarvis (2000), Simulation of water retention and hydraulic conductivity in soil using a three-dimensional network, *Eur. J. Soil Sci.*, *51*(1), 65–79.

Pedarla, A., A. Puppala, L. Hoyos, S. Vanapalli, and C. Zapata (2012), SWRC modelling framework for evaluating volume change behavior of expansive soils, in *Unsaturated Soils: Research and Applications*, edited by C. Mancuso, C. Jommi, and F. D'Onza, pp. 221–228, Springer, Berlin, Heidelberg.

Perrier, E., M. Rieu, G. Sposito, and G. Marsily (1996), Models of the water retention curve for soils with a fractal pore size distribution, *Water Resour. Res.*, *32*(10), 3025–3031.

Phadnis, H. S., and J. C. Santamarina (2011), Bacteria in sediments: Pore size effects, *Géotechnique Lett.*, *1*(4), 91–93.

Reagan, M. T., and G. J. Moridis (2008), Dynamic response of oceanic hydrate deposits to ocean temperature change, *J. Geophys. Res.*, *113*, C12023, doi:10.1029/2008JC004938.

Sanchez, M., and J. C. Santamarina (2010), Analysis of hydrate bearing sediments using a fully coupled THMC formulation, paper presented at Fifth International Conference on Unsaturated Soils, Barcelona, Spain, 6–8 September.

Stange, C. F., and R. Horn (2005), Modeling the soil water retention curve for conditions of variable porosity, *Vadose Zone J.*, *4*(3), 602–613.

Uddin, M., F. Wright, and D. Coombe (2011), Numerical study of gas evolution and transport behaviours in natural gas-hydrate reservoirs, *J. Can. Pet. Technol.*, *50*(1), 70–89.

Vanapalli, S. K., D. G. Fredlund, D. E. Pufahl, and A. W. Clifton (1996), Model for the prediction of shear strength with respect to soil suction, *Can. Geotech. J.*, *33*(3), 379–392.

van Genuchten, M. T. (1980), A closed-form equation for predicting the hydraulic conductivity of unsaturated soils1, *Soil Sci. Soc. Am. J.*, *44*(5), 892–898.

Vogel, H. J. (2000), A numerical experiment on pore size, pore connectivity, water retention, permeability, and solute transport using network models, *Eur. J. Soil Sci.*, *51*(1), 99–105.

Vogel, T., and M. Cislerova (1988), On the reliability of unsaturated hydraulic conductivity calculated from the moisture retention curve, *Transport Porous Media*, *3*(1), 1–15.